In situ X-ray tomography investigation on damage mechanisms in short glass fibre reinforced thermoplastics: Effects of fibre orientation and relative humidity

H. Rolland [a, *], N. Saintier [a], P. Wilson [a, b], J. Merzeau [a], G. Robert [c]

[a] *I2M, Arts et Metiers Paris Tech, Esplanade des Arts et Metiers, 33405 Talence, France*
[b] *Renault S.A.S, 1 Avenue du Golf, 78084 Guyancourt, France*
[c] *Solvay Engineering Plastics, Avenue Ramboz, BP 64, 69192 Saint-Fons, France*

A B S T R A C T

Damage mechanisms of reinforced polyamide 6,6 have been studied in 3D through *in situ* X-ray tomography tensile tests. 3D pictures of the microstructure have been taken during tensile tests to catch damage evolution in the bulk of material. The effects of relative humidity and orientation sampling are particularly investigated in this paper. Main mechanisms have been identified such as fibre failure, debonding, damage at fibre ends and matrix damage (cavitation, fibrillation, damage growth). Qualitative observations reveal that the mechanisms are very sensitive to orientation sampling and relative humidity of the specimen. A specific procedure was developed to propose a quantitative analysis of the results. This analysis shows that identified mechanisms not only have different proportions but also have different kinetics according to relative humidity and orientation sampling of the specimen.

Keywords:
Thermoplastic resin
Microstructures
Damage mechanics
Injection moulding
X-ray microtomography

1. Introduction

Automotive constructors having to reduce the global weight of vehicles, the need of low cost materials with a good ratio density-performances has been growing over the past ten years. Short glass fibre reinforced (SGFR) thermoplastics are good candidates but their behaviour still has to be further understood and modelled in order to be efficiently and widely used. In addition of providing good mechanical properties, SGFR thermoplastics are adapted to moulding injection process, which allows short process cycles, high dimensional precision and complex shapes, well-suited for industrial applications. However, this process induces strong anisotropy through fibres orientation: during injection, the matrix flow field drives fibres orientation.

To evaluate the anisotropy of the material, specimens are usually extracted from injection moulded sheets with different orientations compared to the main injection direction. The effect of the specimen orientation on the macroscale mechanical properties has already been widely studied in literature. For instance, it has been shown that ultimate tensile strength [1] or elastic modulus [2,3] depends on fibre orientation. Mechanical properties anisotropy is strongly linked to different damage kinetics and mechanisms depending on the specimen orientation with respect to the applied mechanical loading [4].

For reinforced polymers, damage is the main source of mechanical properties degradation and has to be precisely described and understood in order to model accurately their behaviour. The works of Sato [5,6] and Horst [7,8] opened the way of local analysis of damage initiation during tensile and fatigue testing. Using SEM fractography and acoustic emission, they observed different damage mechanisms and have elaborated qualitative scenarii for their evolution. From their results, the following main steps for tensile damage were identified: 1) initiation of interfacial microfailure at the fibre ends, 2) propagation of interfacial microfailure along fibre sides, 3) occurrence of plastic deformation band in matrix region, 4) crack opening and slow crack propagation, 5) fast crack propagation. However this description results from surface observations and since this material has a complex 3D microstructure, it has to be completed by volumetric observations. This approach began to be explored thanks to the improvement of observation means such as X-ray tomography. For instance, recent works of Arif et al. [9] combined X-ray tomography and *in situ* SEM bending, in order to

* Corresponding author.
E-mail address: heloise.rolland@ensam.eu (H. Rolland).

http://dx.doi.org/10.1016/j.compositesb.2016.10.043

understand the link between damage mechanisms at the micron scale and the degradation of macroscopic properties. With the same observation strategy, Arif et al. [10] also studied the influence of relative humidity (RH) on the damage mechanisms. This qualitative analysis demonstrated that damage mechanisms at the fibre-matrix interface are more developed when the relative humidity is higher. If it has been noted that the macroscopic properties of the polyamide 6,6 are very sensitive to conditioning [11,12], only a few study evaluate the effects of relative humidity (RH) on the damage mechanisms at the local scale and none really evaluate these effects on their proportions and on their kinetics at the local scale.

It is well admitted that the detrimental effect of water absorption on the mechanical properties of the polyamide is due to polar amide groups. In dry as moulded state, these amide groups constitute strong interactions between crystalline and amorphous phases, by the generation of hydrogen bonds. However, when the polyamide is conditioned at higher RH, amide groups of the amorphous phase interact with water molecules. Consequently, hydrogen bonds are weakened, which increases chain mobility in the amorphous phase: this is the plasticization effect. Properties of the polymer are affected by this plasticization: the glass transition temperature is reduced, as the strength and the modulus, whereas ductility is increased.

In this work, *in situ* microtomography tensile tests were performed to identify the damage mechanisms of short glass fibre reinforced polyamide 6,6. Specimens have been conditioned at three different relative humidity conditions: RH = 0%, 50% or 80% and extracted following three orientations compared to the main flow direction: 0°, 45° or 90°. The first part of this work was to determine the best strategy to adopt for the use of X-ray microtomography to evaluate damage mechanisms in such materials. The results of this preliminary work [4] show that this approach allows to localise damage markers, to obtain their morphology and to differentiate the observed mechanisms. A statistical study led to the evaluation of individual damage mechanisms kinetics under uniaxial tensile tests. In the present work, a similar approach has been applied to specimens with different relative humidity states to represent conditions where the material is in glassy, glass transition and rubbery states. Indeed, modifying the relative humidity shifts the glass transition temperature so that different material state can be reach while testing specimens at ambient temperature. The damage mechanisms are identified and compared in each case. The conclusions provide damage scenarii that consider the effect of the sampling orientation and the relative humidity content for the PA66GF30 composite material, providing quantitative experimental data for micro-mechanical models identification.

2. Experimental procedure

2.1. X-ray microtomography

X-ray microtomography is a non-destructive and high resolution tool based on local attenuation evaluation, which allows to take 3D pictures in the core of materials [13,14]. Its use is an opportunity to understand damage mechanisms in a large variety of materials. This method has recently been applied for SGFR thermoplastics [4,9,15,16] with different uses and interests.

Experiments presented in this work were performed on ID19 beamline at the European Synchrotron Radiation Facility (Grenoble, France). The set-up parameters for these tests were the same as in Ref. [4]: a monochromatic X-ray beam with 194.77 *mA* intensity and 19 *keV* photon energy was used. 2000 radiographs with an exposure time of 0.2 *s* have been received by a Fast Readout Low Noise (FReLoN) 14-bit CCD camera with 2048 × 2048 pixels, during rotation of the machine over 180° along vertical axis. This experimental set-up was optimized to obtain a voxel edge size of 0.7 μm. The acquisition of a complete scan lasts about 9 min.

2.2. Compact tensile machine

A displacement controlled and force measuring machine was developed. One of the key factors regarding 3D image quality is the distance between the specimen and the CCD sensor. The tensile machine was designed to minimize that distance (less than 30 *mm*). The loading ring was made of a 2 mm thickness PMMA tube in order to reduce additional attenuation by the experimental set-up. The machine was directly mounted on the rotating stage of the beam line as shown on Fig. 1. A load cell was specifically designed and an optical camera was synchronised to the data acquisition system in order to capture the specimen deformation at different loading stages. The machine maximum load capacity is 2 *kN* and the displacement is controlled with 0.35 *mm* increments.

2.3. Specimen

The studied material is a Technyl®A218V30, a commercial grade of polyamide 6,6 reinforced by 30 wt% of short glass fibre, supplied by Solvay Engineering Plastics-France. Specimens are sampled from rectangular plates with a 3.24 *mm* thickness, obtained by injection moulding. The injection moulding process leads to an heterogeneous orientation of fibres in the thickness of the plates. This structure is usually described as a superposition of distinguishable layers: the skin, the shell and the core, as illustrated in Fig. 2.

The skin layer is due to the thermal shock between the injected material and the mould walls. Fibres are frozen in their position and orientation forming a 100 μm thick layer of randomly oriented fibres. The shell layer is the largest with a thickness of 1.4 *mm*. In this layer, the shear stress induced by the material flow orientates fibres in the mould flow direction (MFD). The core layer is 300 μm thick in the centre of the specimen. Contrary to the shell, fibres in the core are perpendicular to the MFD. This orientation is due to an

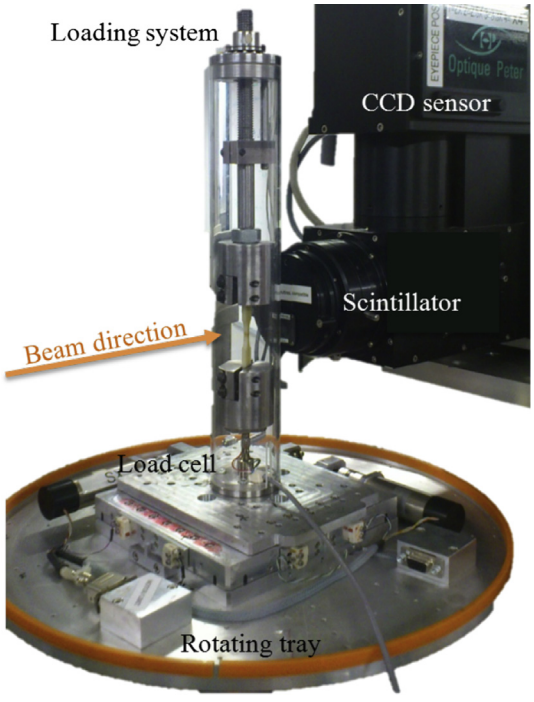

Fig. 1. Compact tensile machine set up [4] for *in situ* testing at ESRF ID19.

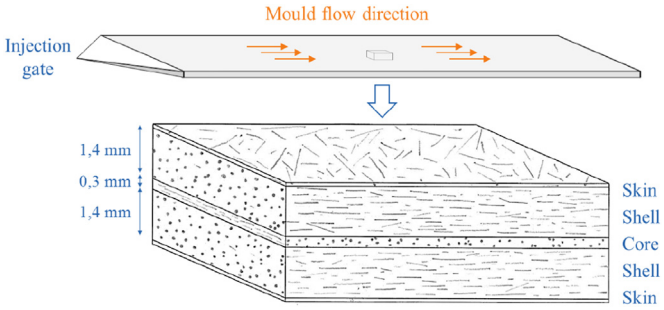

Fig. 2. Core - shell -skin structure in the thickness of the specimen.

extensional flow during the injection process and induces a rotation of the axes of orthotropy in the thickness of the specimen.

2.3.1. Orientation

Samples were extracted following three different orientations compared to the main injection direction: 0°, 45° and 90°, as presented in Fig. 3.

2.3.2. Geometry

The specimen geometry was designed to accommodate the constraints of the experimental set-up. Indeed, 3D X-ray microtomography only allows to observe relatively small volumes, depending on resolution and sensor size. The synchrotron experimental set-up described in the previous section allows to obtain a cylindrical observed zone of 1.4 *mm* diameter and 1.4 *mm* height (2048 pixels x 0.7 μm resolution). The gage length was designed so that the stress state in the observed volume was homogeneous and a square section was chosen to improve microtomography quality (compared to a rectangular section). Taking into account these elements, the geometry of the specimen was chosen as presented in Fig. 3. This geometry allows to obtain similar tensile tests results as on full scale normalised tensile specimens obtained by the same process.

2.3.3. Conditioning

The conditioning of the specimens have led to equilibrium humidity content corresponding to three different relative humidity conditions, i.e. RH = 0%, 50% and 80%. RH0 specimens correspond to dry as moulded specimens. RH50 and RH80 specimens are put in a chamber at 70 °C, respectively at RH = 62% and RH = 80% of humidity until their water uptake stabilization. Then, RH50 specimens pass 15 days at 23 °C, RH = 50%, when RH80 specimens are kept at 30 °C, RH = 80%. It is worth noting that the water uptake does not affect the fibre orientation distribution. The water uptake of the polyamide is a reversible process, it can be thus reduced or increased, depending on the environmental (RH, temperature) conditions. Therefore, ensuring the material RH stability before and during testing is important. After conditioning, specimens were sealed in individual packets to prevent any change in RH. Each packet was opened just before testing. Considering the short duration of each experiment (less than 1h30), the water content was considered as constant between the beginning and the end of the tensile tests.

2.4. 3D image processing

2.4.1. Thresholds choice on grey levels

Each voxel forming the 3D picture is defined by a position and a grey level which corresponds to the density of the represented matter. In the present case, the grey intensity of the voxel indicates if it belongs to fibre, matrix or damage marker phases. To process tomography data, thresholds on grey levels that will allow to separate the different phases, have to be chosen. The grey level histograms corresponding to each loading step, RH and orientation are plotted in Fig. 4. Histograms of all scans have been superposed in order to identify thresholds for the different phases. Two peaks appear on the diagrams, one corresponding to the fibres (grey levels around 36000) and the second one to the matrix. Due to slight modification of the brightness of the acquired scans, the grey level histograms were slightly corrected in order to have a similar position of the peak corresponding to the fibre phase. Only brightness (offset of the histogram), was modified with a maximum shift of 1500 grey levels over 64000 grey levels in total, contrast being kept as constant (no dilatation of the histogram). After this process, it is worth noting that the position of the matrix and fibre peaks are identical for all loading step, RH and orientation configurations.

Several approaches are possible to determine phases thresholds. For instance, Cosmi [17] formalised a method based on the identification and statistical repartition of the matrix grey-tone range in the histogram. Here, the choice for the grey threshold defining the fibre phase is motivated by direct visual determination on the 3D

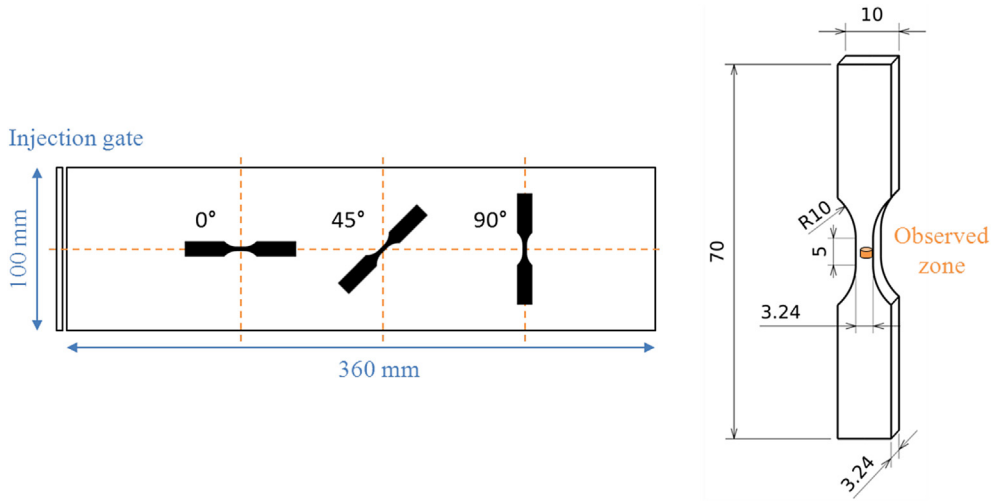

Fig. 3. Specimen sampling from injected plates and geometry for *in situ* tensile tests.

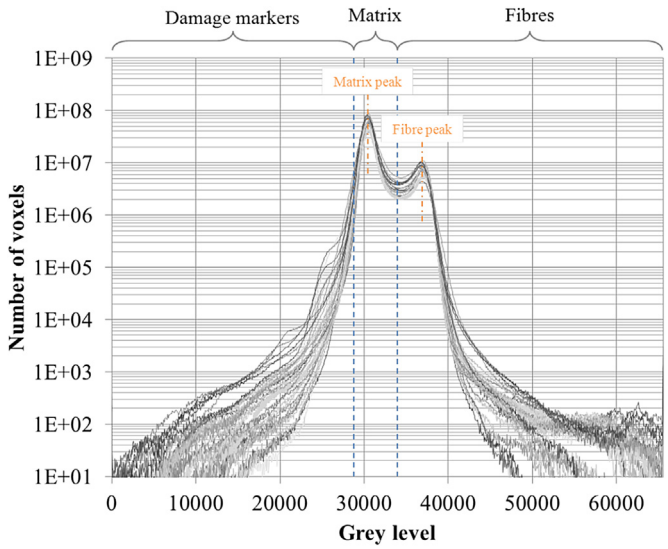

Fig. 4. Number of voxels per grey level at different stress levels for all specimens.

images. The influence of the threshold between damage and matrix has then been cautiously analysed, as shown in Fig. 5. From this analysis, using 16 different threshold values and strengthened by observations on all scans, the threshold has been fixed at 29200 for all scans. It has to be noticed that this threshold corresponds to a local minimum on the volume/grey level curve given in Fig. 5, so that if a slight brightness offset still exists in between different scans, it is considered to have a limited impact on the identified damage phase.

2.4.2. Data treatments

After the application of the chosen threshold, the picture is divided in voxels of fibre, matrix or damage markers. A damage marker is defined as a group of voxels having a face, an edge or a corner in common, in order to foster the connection between zones damaged by the same local effect. Then, each object is described by coordinates of its barycentre, length (Feret diameter), width (inner diameter), aspect ratio (*Length*/*Width*), volume and orientation (defined by the axis of minimum inertia). A fibre is defined as a group of voxels having, at least, one shared face, in order to facilitate fibres separation. In order to improve the object separation, different image processing are possible, depending on phase shapes, volumetric fractions and phase contrast. Here, damage markers have been analysed directly after the threshold step contrary to fibres, for which it is necessary to apply a sequence of filters (opening, erosion, separation and dilatation) in order to reach the most accurate description of this phase.

3. Results

3.1. Overall mechanical properties

Strain/stress curves are presented in Fig. 6(a) and (b) and 6(c), according to their humidity rate and orientation sampling. At this scale, both effects of the conditioning and of the orientation sampling can be noticed. The observed effect of fibre orientation on the mechanical properties (tensile strength, ductility) are consistent with already published results. At fixed orientation, the effect of humidity is to reduce the tensile strength (minus 45% from RH0 to RH80) and increase the ductility (plus 33% from RH0 to RH80).

3.2. Damage mechanisms identification with observations at the micron scale

Taking into account all specimens, six elementary damage mechanisms have been observed and will be described in the following paragraphs. One mechanism directly concerns fibres (fibre failure). Two mechanisms are related to the fibre-matrix interface (debonding and damage at fibre ends), three mechanisms are related to the matrix (cavitation, fibrillation and damage growth). First the elementary mechanisms will be described and illustrated, then a quantitative analysis depending on the orientation and conditioning of the specimen will be proposed.

3.2.1. Fibre failure

In a previous work [4], a high level of fibre failure in the whole gage length was evidenced, while this mechanism was largely underestimated in previous studies (more than one fibre over four is broken at the end of tensile tests). This mechanism is observed soon in the tensile test: at lower stress levels, failures happen at crossing between fibres, due to local overstress induced by fibre crossing. Different failure modes have been observed, but typically, fibres fail as shown in Fig. 7. It also has to be noticed that a fibre can fail in several parts, that considerably reduce the effective fibre length as the stress level increases.

Fig. 8 presents a typical fibre failure in specimens with different conditioning. This comparison indicates that relative humidity

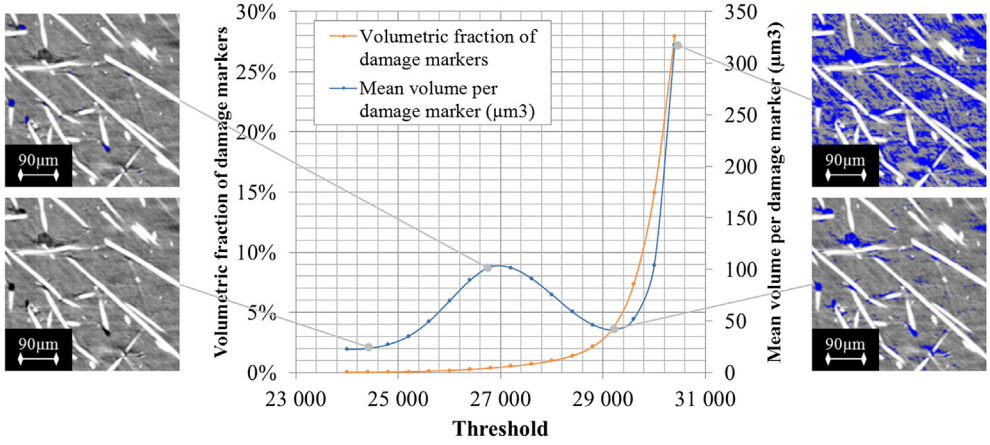

Fig. 5. Effect of threshold choice on damage markers volume on one specimen (RH50 45° specimen).

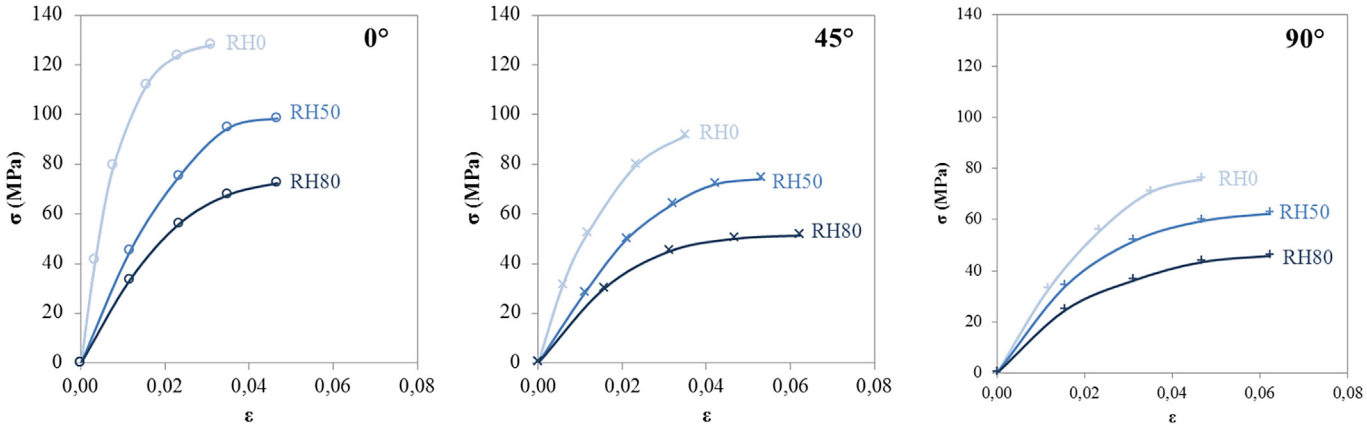

(a) 0° oriented specimens (b) 45° oriented specimens (c) 90° oriented specimens

Fig. 6. Experimental engineering stress and total strain for each test.

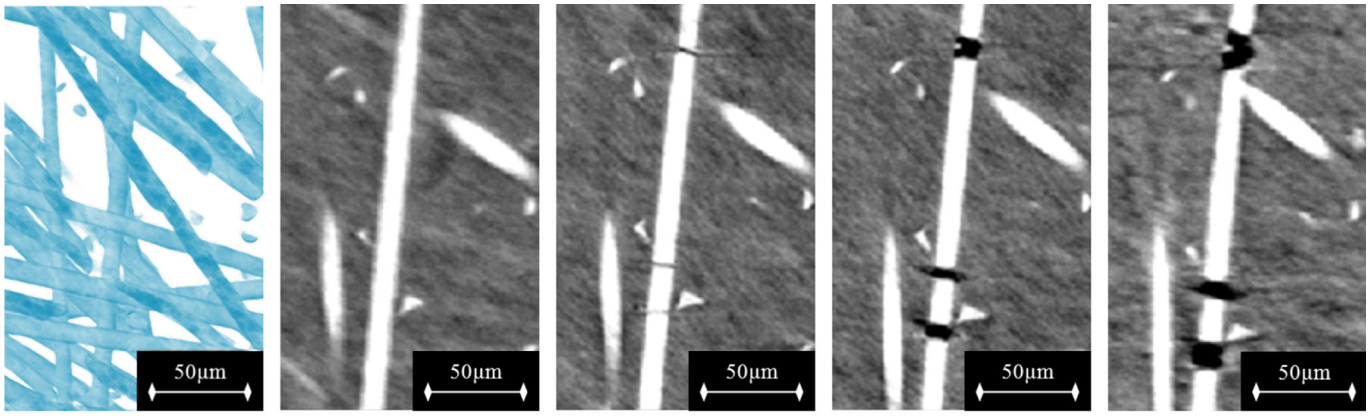

(a) Initial fibres configuration (b) $\varepsilon_1 = 0.0\%$ $\sigma_1 = 0.0$ MPa (c) $\varepsilon = 2.1\%$ $\sigma = 49.7$ MPa (d) $\varepsilon = 4.2\%$ $\sigma = 71.9$ MPa (e) $\varepsilon = 5.3\%$ $\sigma = 74.1$ MPa

Fig. 7. Fibre failure - RH50 45° specimen.

mainly influences the aspect of a marker after the failure, making detection easier for specimens with higher relative humidity. Indeed, since the failure of the fibre is mostly a stress driven phenomenon, for the same specimen orientation, fibre failure and fragmentation are found to be very similar at the same macroscopic stress. However, due to matrix softening at high relative humidity, the deformation induced by stress/strain redistribution around the broken fibre is much higher at higher relative humidity.

3.2.2. Damage at fibre ends

Fig. 9 illustrates the evolution of damage at fibre ends, for a 45° specimen, conditioned at RH50. This mechanism is the first to appear during the tensile test and is present in the whole gage length. At the onset of failure, it can affect one third of fibres in dry specimen and over half of fibres in conditioned specimens. Two main reasons can explain this damage mechanism: the poor fibre-matrix adhesion properties at fibre ends because of absence of sizing, as previously mentioned in the literature [4,8,18,19] and the fibre geometry, turning fibre ends into stress concentrators. At initiation, the length of the damage marker is linked with the diameter of the fibre, as presented in Fig. 10. Then, for conditioned specimens (RH50 and RH80), it extends in the macroscopic tensile direction and progressively expands spherically, due to the local stress state and matrix ductility. Close to the failure, the mode of expansion changes, switching to a damage growth in the matrix (see paragraph 3.2.6). For dry specimens (RH0), this extension is restricted to small volumes. Damage at fibre ends mechanism is observed in all specimens, even at fibre ends in 90° oriented specimens, as illustrated in Fig. 11. Indeed the key parameter for initiating damage at fibre end is the normal stress acting on the fibre end face. Two main reasons explain why fibre end damage can still be initiated at 90° specimens: 1) fibres are, in average, oriented at 90° but a significant amount of fibres are off axis and are between 80° and 110°, 2) during process, fibres break, resulting faces are not strictly perpendicularly to the fibre axis but rather at 40–45° with respect to it.

3.2.3. Debonding

Debonding initiates at advanced steps in the tensile test, corresponding to high levels of stress. Debonding on one fibre is often triggered on by an adjacent fibre end that induces stress concentration at this scale or by close crossing fibres that induce matrix confinement. Both configurations induce local stress concentration that promotes interface debonding. As shown in Fig. 12, the local stress relaxation at fibre-matrix interface and asymmetry induced by the debonding may lead to high distortion of the fibre. The relative humidity does not seem to influence qualitatively this mechanism, as illustrated in Fig. 13. Hence, the confinement of the

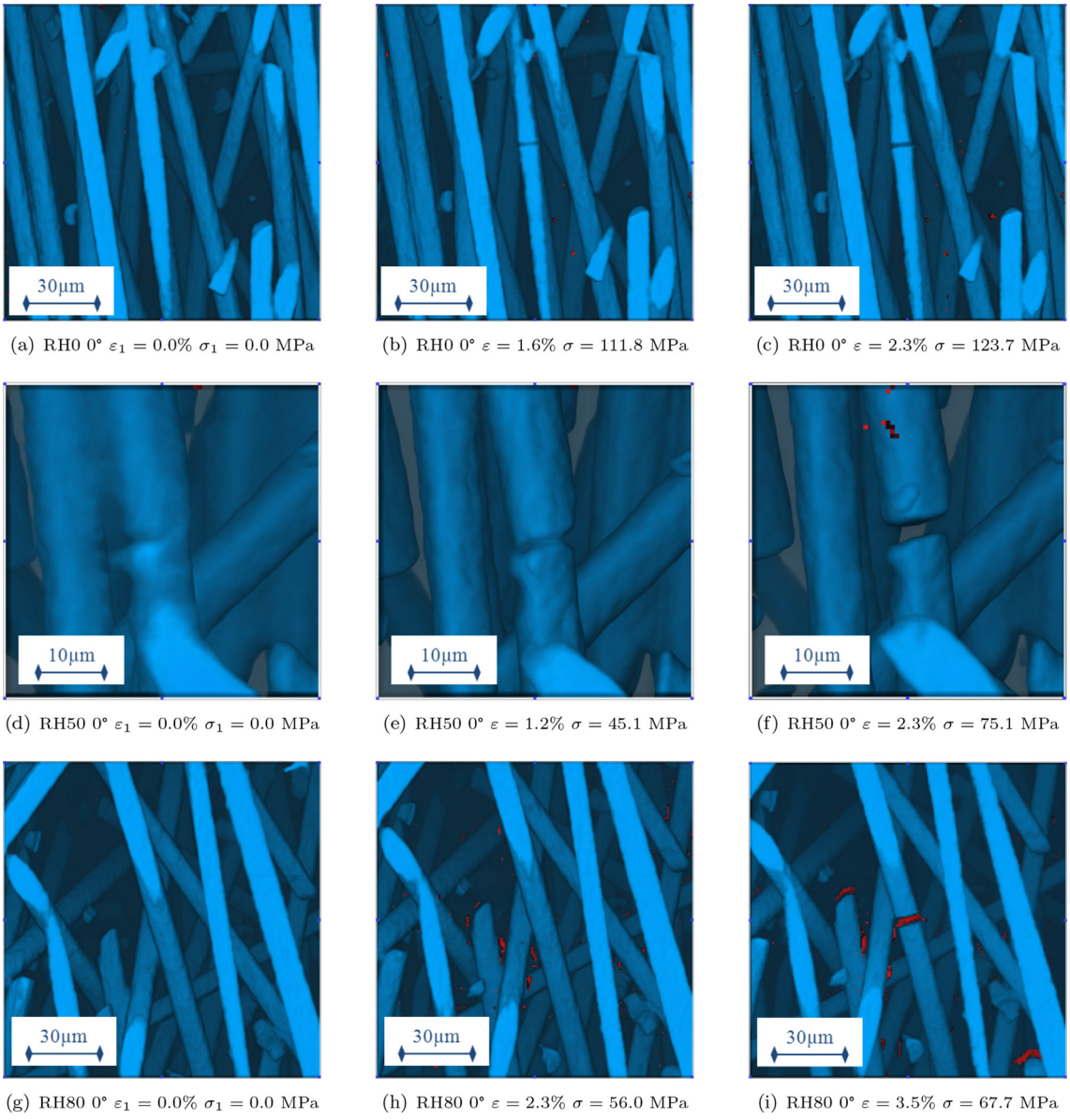

(a) RH0 0° $\varepsilon_1 = 0.0\%$ $\sigma_1 = 0.0$ MPa (b) RH0 0° $\varepsilon = 1.6\%$ $\sigma = 111.8$ MPa (c) RH0 0° $\varepsilon = 2.3\%$ $\sigma = 123.7$ MPa

(d) RH50 0° $\varepsilon_1 = 0.0\%$ $\sigma_1 = 0.0$ MPa (e) RH50 0° $\varepsilon = 1.2\%$ $\sigma = 45.1$ MPa (f) RH50 0° $\varepsilon = 2.3\%$ $\sigma = 75.1$ MPa

(g) RH80 0° $\varepsilon_1 = 0.0\%$ $\sigma_1 = 0.0$ MPa (h) RH80 0° $\varepsilon = 2.3\%$ $\sigma = 56.0$ MPa (i) RH80 0° $\varepsilon = 3.5\%$ $\sigma = 67.7$ MPa

Fig. 8. Effect of relative humidity on fibre failure in 0° specimens.

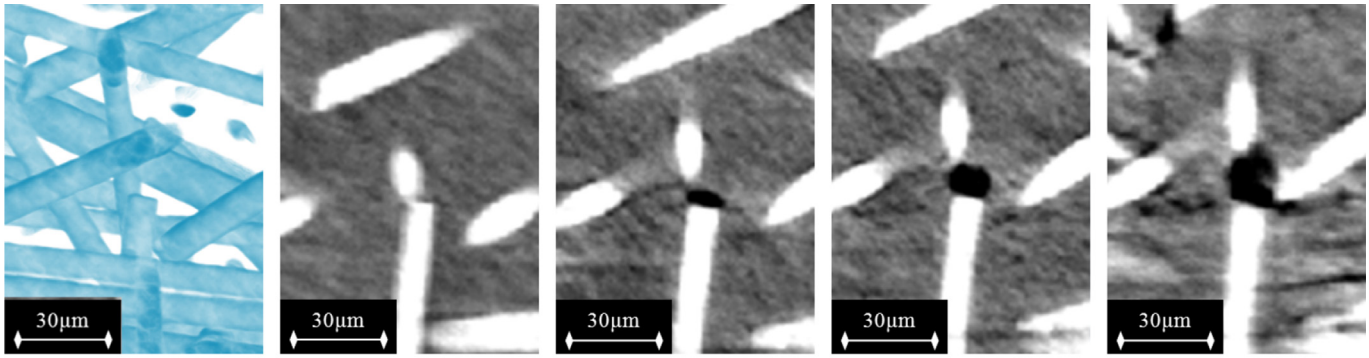

(a) Initial fibres configuration (b) $\varepsilon_1 = 0.0\%$ $\sigma_1 = 0.0$ MPa (c) $\varepsilon = 3.2\%$ $\sigma = 63.9$ MPa (d) $\varepsilon = 4.2\%$ $\sigma = 71.2$ MPa (e) $\varepsilon = 5.3\%$ $\sigma = 74.1$ MPa

Fig. 9. Damage at fibre ends - RH50 45° specimen.

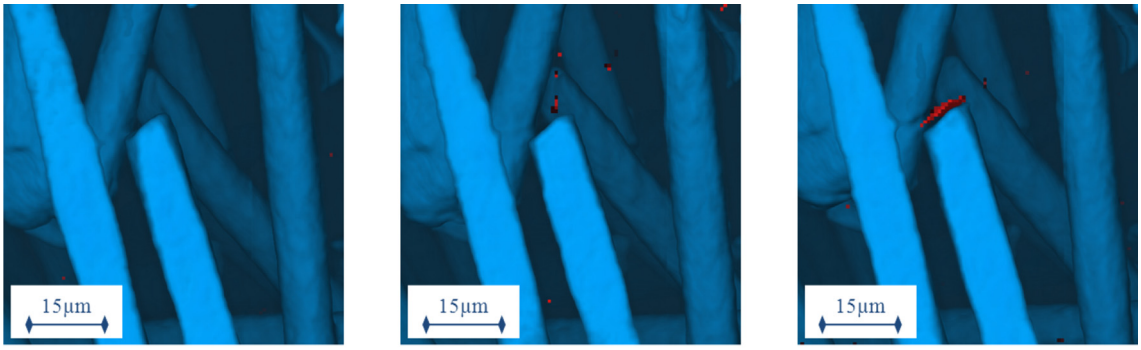

(a) RH0 0° $\varepsilon_1 = 0.0\%$ $\sigma_1 = 0.0$ MPa (b) RH0 0° $\varepsilon = 1.6\%$ $\sigma = 111.8$ MPa (c) RH0 0° $\varepsilon = 2.3\%$ $\sigma = 123.7$ MPa

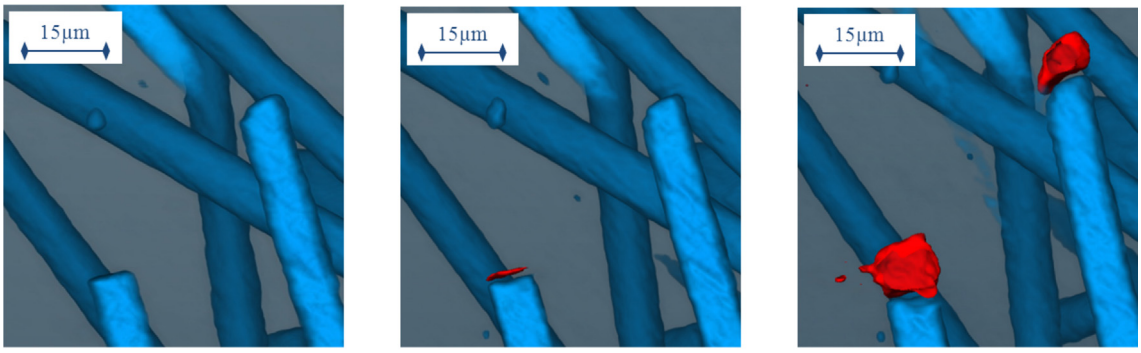

(d) RH50 45° $\varepsilon_1 = 0.0\%$ $\sigma_1 = 0.0$ MPa (e) RH50 45° $\varepsilon = 2.1\%$ $\sigma = 49.7$ MPa (f) RH50 45° $\varepsilon = 4.2\%$ $\sigma = 71.9$ MPa

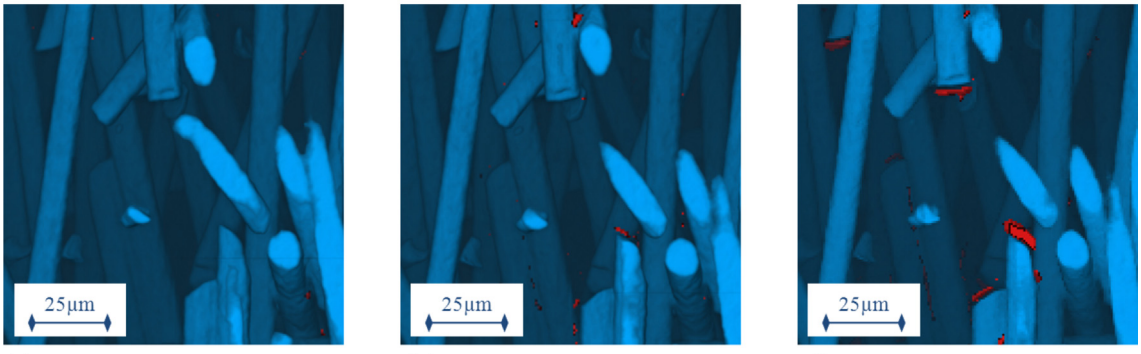

(g) RH80 0° $\varepsilon_1 = 0.0\%$ $\sigma_1 = 0.0$ MPa (h) RH80 0° $\varepsilon = 2.3\%$ $\sigma = 56.0$ MPa (i) RH80 0° $\varepsilon = 3.5\%$ $\sigma = 67.7$ MPa

Fig. 10. Effect of relative humidity on damage at fibre ends.

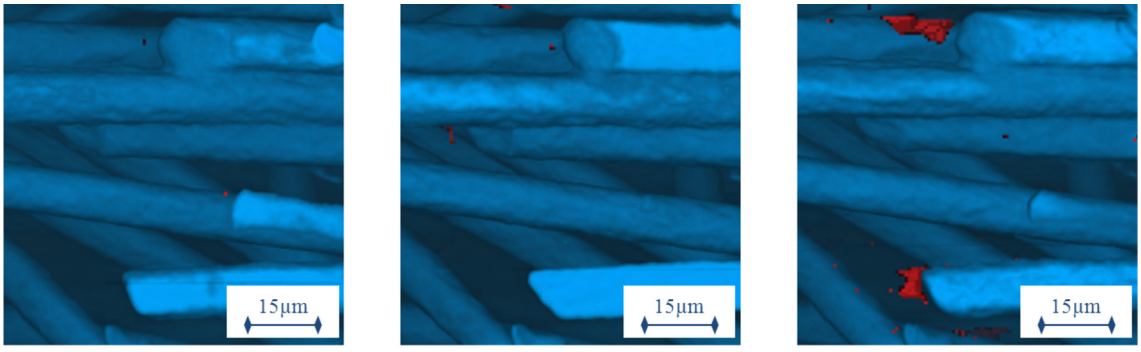

(a) RH0 90° $\varepsilon_1 = 0.0\%$ $\sigma_1 = 0.0$ MPa (b) RH0 90° $\varepsilon = 1.2\%$ $\sigma = 32.6$ MPa (c) RH0 90° $\varepsilon = 2.3\%$ $\sigma = 55.4$ MPa

Fig. 11. Damage at fibre ends in a 90° specimen.

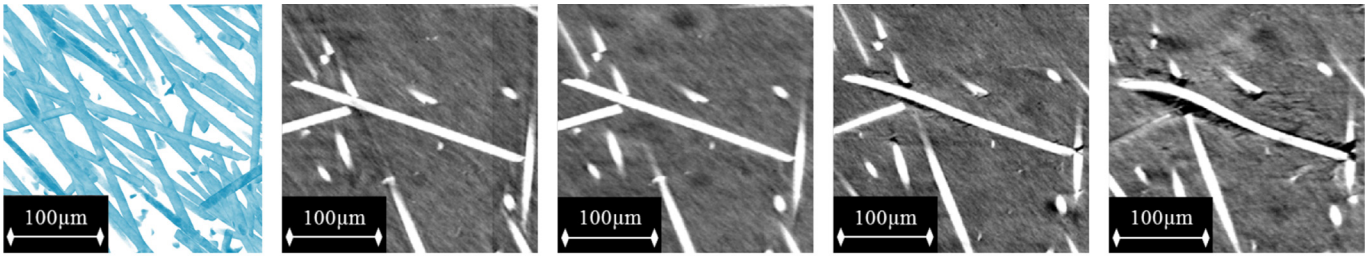

(a) Initial fibres configuration (b) $\varepsilon_1 = 0.0\%$ $\sigma_1 = 0.0$ MPa (c) $\varepsilon = 2.1\%$ $\sigma = 49.7$ MPa (d) $\varepsilon = 4.2\%$ $\sigma = 71.9$ MPa (e) $\varepsilon = 5.3\%$ $\sigma = 74.1$ MPa

Fig. 12. Debonding at the fibre-matrix interface - RH50 45° specimen - Effect of local fibres and confinement on debonding.

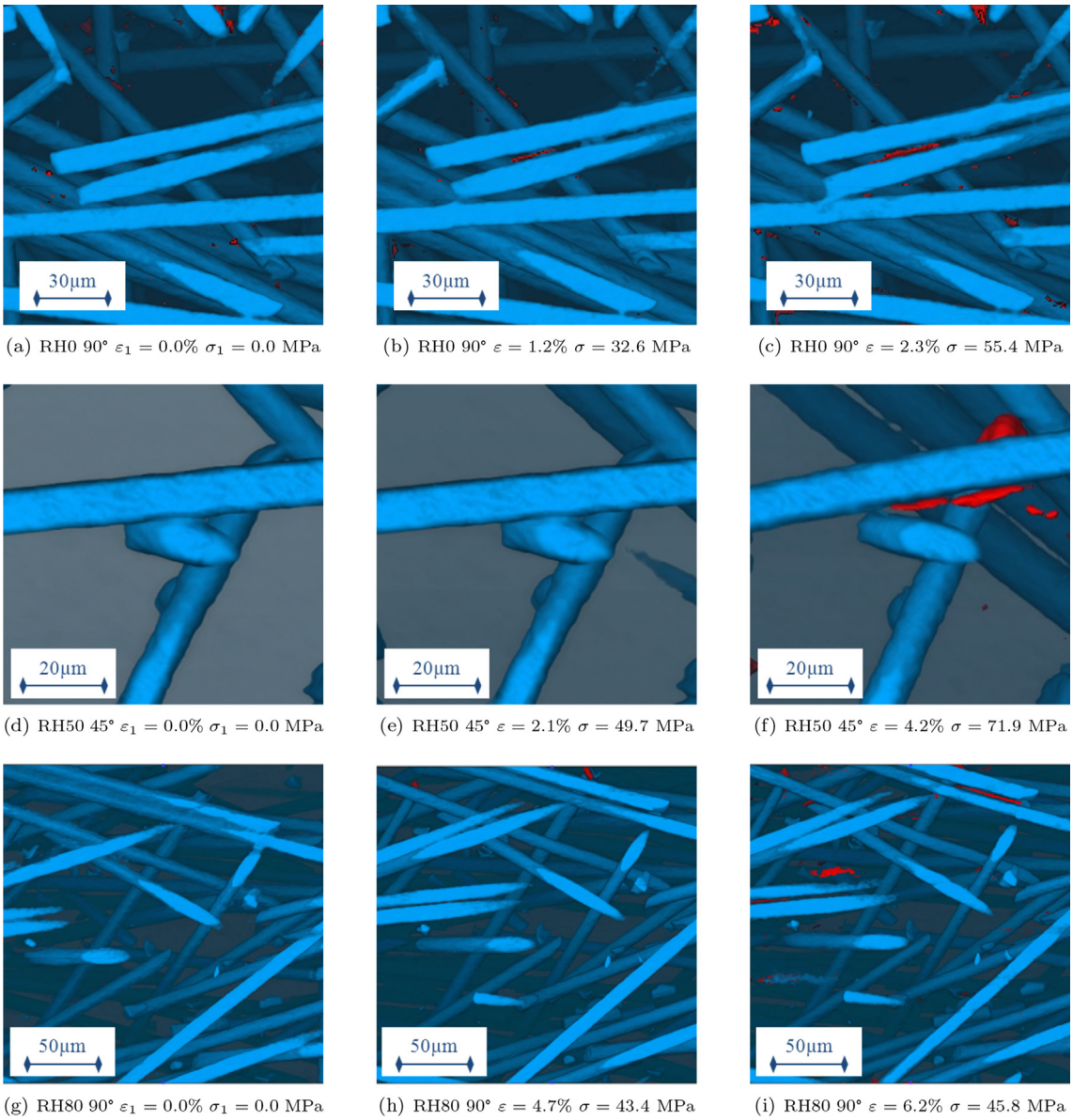

(a) RH0 90° $\varepsilon_1 = 0.0\%$ $\sigma_1 = 0.0$ MPa (b) RH0 90° $\varepsilon = 1.2\%$ $\sigma = 32.6$ MPa (c) RH0 90° $\varepsilon = 2.3\%$ $\sigma = 55.4$ MPa

(d) RH50 45° $\varepsilon_1 = 0.0\%$ $\sigma_1 = 0.0$ MPa (e) RH50 45° $\varepsilon = 2.1\%$ $\sigma = 49.7$ MPa (f) RH50 45° $\varepsilon = 4.2\%$ $\sigma = 71.9$ MPa

(g) RH80 90° $\varepsilon_1 = 0.0\%$ $\sigma_1 = 0.0$ MPa (h) RH80 90° $\varepsilon = 4.7\%$ $\sigma = 43.4$ MPa (i) RH80 90° $\varepsilon = 6.2\%$ $\sigma = 45.8$ MPa

Fig. 13. Effect of relative humidity on debonding.

matrix has a first order importance for the apparition and propagation of this mechanism, before the relative humidity of the specimen and orientation of fibres, as illustrated for 0° oriented specimens in Fig. 14.

Detected markers corresponding to debonding are characterised by an elevated aspect ratio (ratio between the length and the width). Indeed, they are particularly elongated and do not reach large volumes. However, it may impact significantly the overall

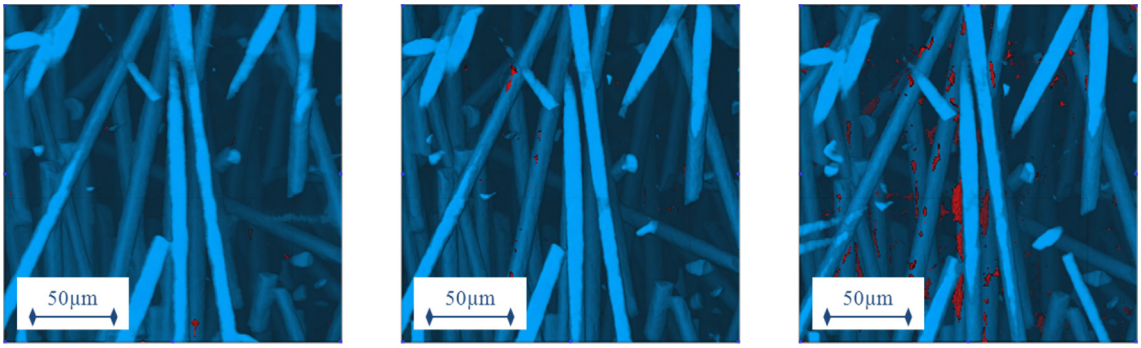

(a) RH50 0° $\varepsilon_1 = 0.0\%$ $\sigma_1 = 0.0$ MPa (b) RH50 0° $\varepsilon = 1.2\%$ $\sigma = 45.1$ MPa (c) RH50 0° $\varepsilon = 2.3\%$ $\sigma = 75.1$ MPa

(d) RH80 0° $\varepsilon_1 = 0.0\%$ $\sigma_1 = 0.0$ MPa (e) RH80 0° $\varepsilon = 2.3\%$ $\sigma = 56.0$ MPa (f) RH80 0° $\varepsilon = 3.5\%$ $\sigma = 67.7$ MPa

Fig. 14. Debonding in 0° specimens.

stress response of the material since it affects directly the fibre-matrix interface and consequently the load transfer from the matrix to the fibre.

If the debonding is precisely located at the interface between the fibre and the matrix, detailed observation of the debonding process evidenced another mechanism, in the matrix at few microns from this interface as shown in Fig. 16. This mechanism corresponds to a degradation (damage) of the matrix near the interface and thus, is described in a following paragraph, associated to a matrix damage process (see section 3.2.4).

3.2.4. Fibrillation

A population of damage markers appears in the form of an arrangement of micro-cracks in the matrix as illustrated in Fig. 15. In addition, these damaged zones appear to be darker than the matrix but lighter than markers linked with other mechanisms, which indicates an intermediate density. Those two characteristics (micro-cracks and intermediate density) let us suppose that such damage markers correspond to a fibrillation phenomenon in the polymer matrix. The intermediate density is associated to the occurrence of fibrils (bridging the two sides of the crack) that can not be resolved with the 0.7 μm resolution of the X-ray micro-tomographic pictures (typical fibrils diameter being around 0.1μm). These markers generally have a pronounced orientation driven by local stress/strain state.

Once again confined areas in the vicinity of packed groups of fibres seems to promote this damage mechanism. The presence of fibrillation is both linked with fibre orientation and conditioning of the specimen. This mechanism only appears for advanced stages of tensile tests (highly strained specimens), in the matrix of specimens with high relative humidity (RH50 and RH80) generally between fibres oriented around 45°. For this reason, this mechanism is particularly widespread in 45° oriented specimens, as illustrated in Fig. 16. This figure also illustrates the sensitivity of this mechanism to the relative humidity: in the matrix next to the interface, some cavitation occurs at few microns from the fibre. The initiated

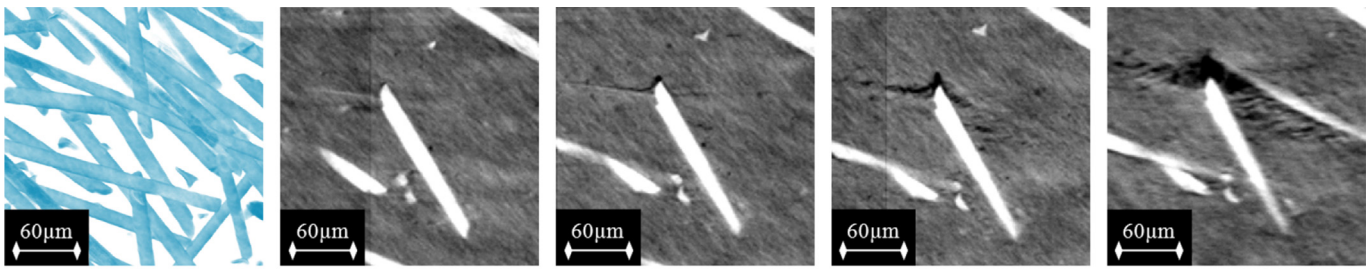

(a) Initial fibres configuration (b) $\varepsilon_1 = 0.0\%$ $\sigma_1 = 0.0$ MPa (c) $\varepsilon = 3.2\%$ $\sigma = 63.9$ MPa (d) $\varepsilon = 4.2\%$ $\sigma = 71.9$ MPa (e) $\varepsilon = 5.3\%$ $\sigma = 74.1$ MPa

Fig. 15. Fibrillation - RH50 45° specimen.

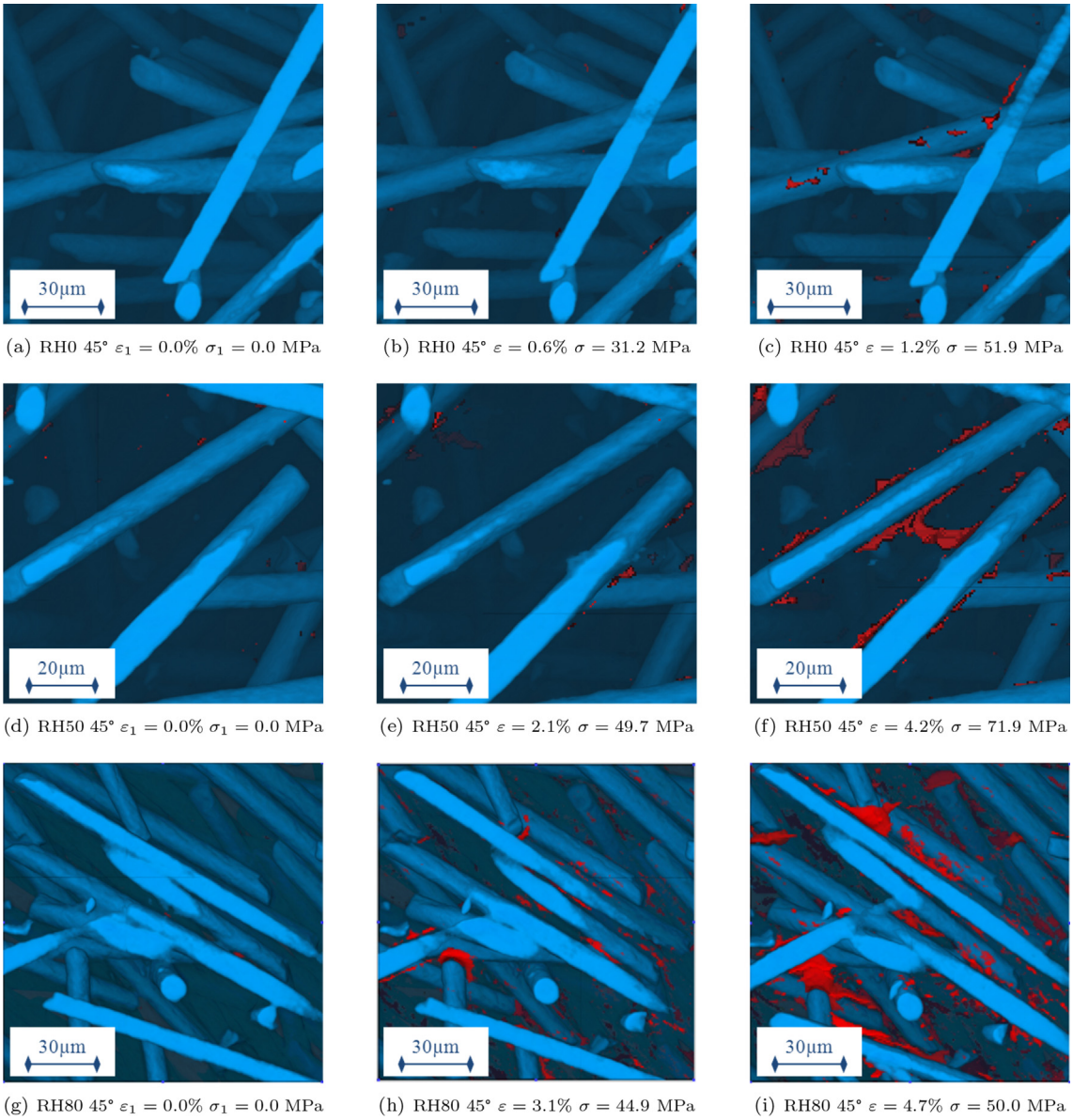

(a) RH0 45° $\varepsilon_1 = 0.0\%$ $\sigma_1 = 0.0$ MPa (b) RH0 45° $\varepsilon = 0.6\%$ $\sigma = 31.2$ MPa (c) RH0 45° $\varepsilon = 1.2\%$ $\sigma = 51.9$ MPa

(d) RH50 45° $\varepsilon_1 = 0.0\%$ $\sigma_1 = 0.0$ MPa (e) RH50 45° $\varepsilon = 2.1\%$ $\sigma = 49.7$ MPa (f) RH50 45° $\varepsilon = 4.2\%$ $\sigma = 71.9$ MPa

(g) RH80 45° $\varepsilon_1 = 0.0\%$ $\sigma_1 = 0.0$ MPa (h) RH80 45° $\varepsilon = 3.1\%$ $\sigma = 44.9$ MPa (i) RH80 45° $\varepsilon = 4.7\%$ $\sigma = 50.0$ MPa

Fig. 16. Effect of relative humidity on fibrillation.

cavities turn into fibrils with a particular orientation resulting from the combination of normal stress induced by the macroscopic loading and shear stress induced by neighbouring fibres. These damage markers with fibrils turn into microcracks that progress in the bulk of the matrix, with deformation increase.

3.2.5. Cavitation

Cavitation appears in the form of small cavities in the matrix, as illustrated in Fig. 17. During *in situ* monotonic tensile tests, most of these cavities are satellites of other damage markers and do not appear as an independent mechanism. Thus, it will be considered that this mechanism is not predominant in the macroscopic failure process, but that it is a good indicator of the global evolution of damage in the gage length.

3.2.6. Damage growth in the matrix

This mechanism refers to the growth of damage markers in the bulk of polymer matrix. It can consist in the expansion of markers with important volumes or in the merging of several markers, taking over from debonding and fibrillation mechanisms. In specimens where this mechanism appears, the scenario is the same: damage is initiated in a zone of confined matrix between close fibres with significant differences in orientations. This fibre configuration results in a stress concentration and drives damage growth. This damage development in the bulk of polymer matrix tends to be spherical and is neither parallel nor transverse to the macroscopic stress direction, probably due to stress triaxiality, as shown in Fig. 18. In the final stages, fibrillation between damage markers seems to significantly participate to damage coalescence.

This mechanism has not been observed for all conditioning-orientation combinations (absent of 0° or dry specimens). Resulting from the growth of existing damage zones such as debonding and fibrillation, it is due to the combination of local fibre configuration and matrix in the rubbery state. In addition it was only observable at the ultimate stages of the tensile test, as illustrated in Fig. 19.

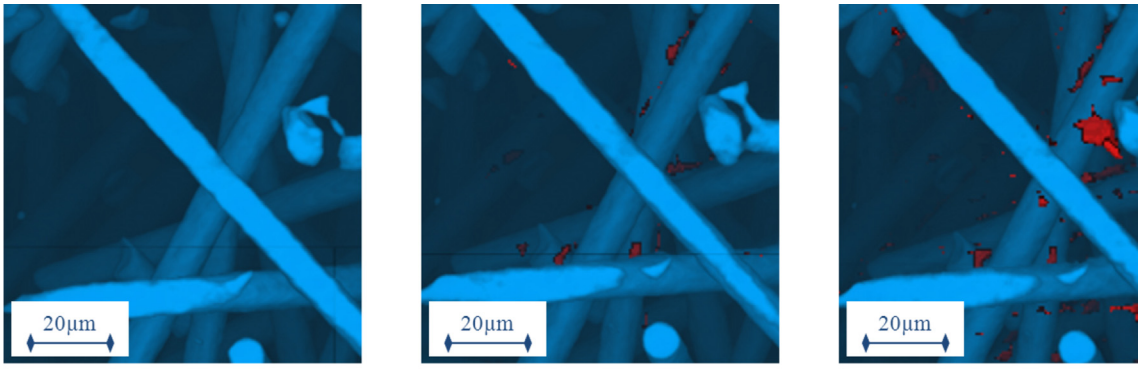

(a) RH0 90° $\varepsilon_1 = 0.0\%$ $\sigma_1 = 0.0$ MPa (b) RH0 90° $\varepsilon = 1.2\%$ $\sigma = 32.6$ MPa (c) RH0 90° $\varepsilon = 2.3\%$ $\sigma = 55.4$

Fig. 17. Cavitation process.

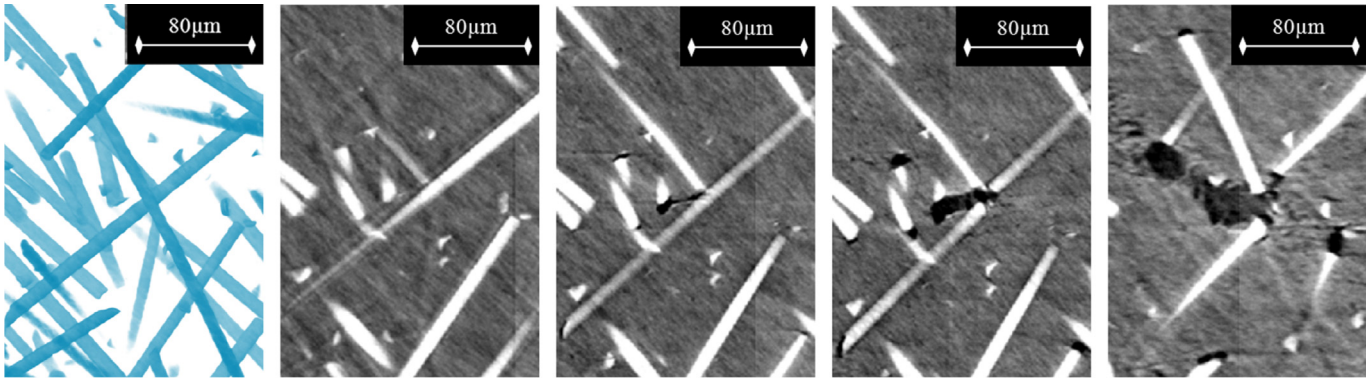

(a) Initial fibres configuration (b) $\varepsilon_1 = 0.0\%$ $\sigma_1 = 0.0$ MPa (c) $\varepsilon = 3.2\%$ $\sigma = 63.9$ MPa (d) $\varepsilon = 4.2\%$ $\sigma = 71.9$ MPa (e) $\varepsilon = 5.3\%$ $\sigma = 74.1$ MPa

Fig. 18. Damage growth in the matrix - RH50 45° specimen.

3.3. Analysis at the specimen scale

3.3.1. Classification of markers to each damage mechanism

From the different observations, it is possible to deduce the typical morphology of a marker according to a damage mechanism. A classification of these markers has been made, based on three measures: the length, the aspect ratio and the volume. According to observations, damage growth in the matrix is the mechanism that corresponds to all markers with an important volume. Cavitation concerns small markers, so is represented by markers with a small length. Debonding is linked with elongated markers, thus a high aspect ratio. Fibrillation is associated with markers whom length is largely superior to a fibre diameter whereas fibre failure and damage at fibre ends are close to this length. Finally, a distinction between these two last mechanisms is proposed by considering a lower aspect ratio for markers at fibre ends, which tend to be more spherical. A similar approach was proposed in Ref. [4], the only difference being the addition of the fibrillation phenomena that is more clearly evidenced on this set of results on conditioned specimens.

The different thresholds to classify the markers have been estimated from the microscopic observations. Fig. 20(a) presents the thresholds used for this classification. A scan that exhibits all mechanisms during observations, has been chosen to illustrate this classification. This is the case of the fourth scan obtained on the specimen oriented at 45° and conditioned at 50% of relative humidity. The diagram 20(b) and the picture 20(c) are the results of the application of the determined limits on this scan. The visualisation of the classification in the gage length allows to check the consistence with observations and then, to validate the quantitative exploitation of the resulting data.

3.3.2. Effect of specimen orientation and conditioning on damage mechanisms

To describe kinetics and evolution of the six identified mechanisms during tensile tests, different measures per mechanism have been extracted: the density, the volumetric fraction of damage markers, the distribution of markers orientation. It should be noticed that for damage markers with low aspect ratio, the orientation may not be meaningful and will not be analysed.

3.3.2.1. Fibre failure and damage at fibre ends. The quantitative analysis presented a fibre density of around 9,000$fibres/mm^3$ for all the specimens, with a fibre length distributed between 20 and 800 μm. Fibre failure and damage at fibre ends kinetics are similar. These mechanisms are the first to be activated during tensile test, whatever the orientation or the conditioning. Nevertheless, the proportion of fibres affected by these mechanisms depends on the specimen orientation and conditioning, as presented in Figs. 21 and 22. For dry specimens, the orientation sampling has a high influence on damage at fibre ends density: only 1/20 of fibres is concerned for 0° specimen, whereas 1/10 and 1/6 of fibre ends are respectively damaged for 45° and 90° specimens. On the other hand, in conditioned specimens, the orientation sampling has no influence: in the three cases, a quarter of fibres are concerned by this mechanism. As described in the paragraph 3.2.2, orientation of

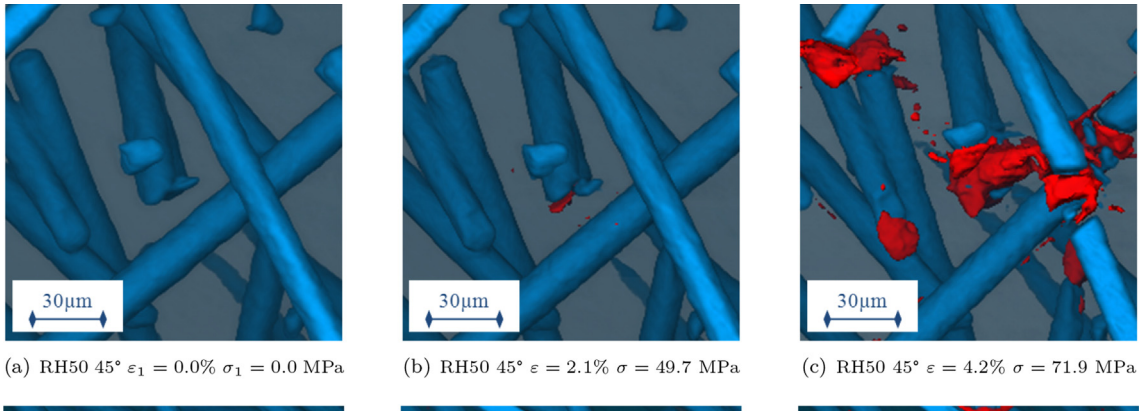

(a) RH50 45° $\varepsilon_1 = 0.0\%$ $\sigma_1 = 0.0$ MPa (b) RH50 45° $\varepsilon = 2.1\%$ $\sigma = 49.7$ MPa (c) RH50 45° $\varepsilon = 4.2\%$ $\sigma = 71.9$ MPa

(d) RH80 45° $\varepsilon_1 = 0.0\%$ $\sigma_1 = 0.0$ MPa (e) RH80 45° $\varepsilon = 3.1\%$ $\sigma = 44.9$ MPa (f) RH80 45° $\varepsilon = 4.7\%$ $\sigma = 50.0$ MPa

Fig. 19. Damage growth in the matrix depending on the RH (not observed in RH0 specimens).

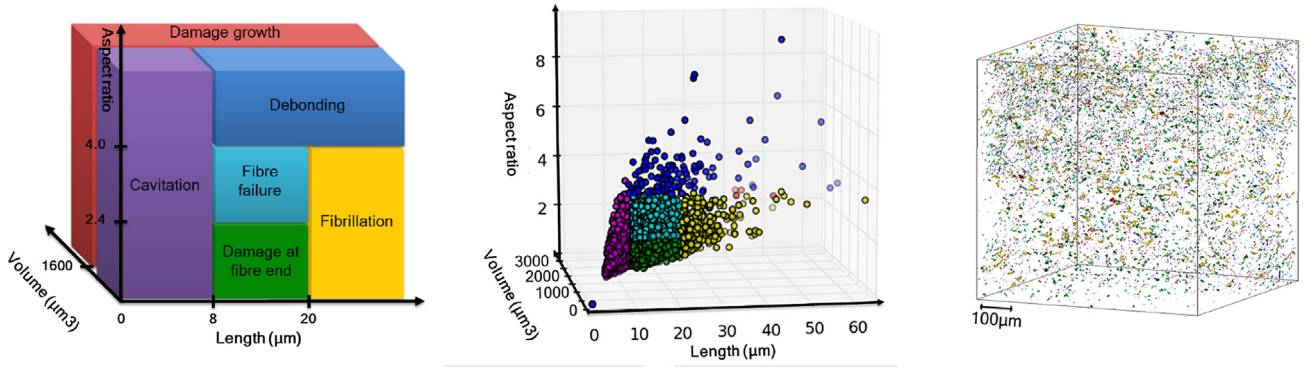

(a) Limits for the classification of markers (b) Length - Aspect Ratio - Volume diagram of classified markers (c) Classified markers in the gage length

Fig. 20. Classification of damage markers.

the fibre end face prevails over fibre orientation, that explains the development of damage at fibre ends in conditioned specimens with different orientations. This is also consistent with spread orientations of damage markers around fibre orientation presented in Fig. 23.

3.3.2.2. Debonding. The density of debonding markers is four to ten times lower than the density of damage markers at fibre ends. Also, this mechanism is activated for higher stresses, due to the geometry of fibres and presence of sizing along fibre sides. This mechanism is highly influenced by specimen orientation: 90° oriented specimens reach the same high density of debonding, whatever their conditioning, as shown in Fig. 24. For 45° oriented specimens, debonding is twice denser for the specimen in a rubbery state. Concerning 0° oriented specimens, debonding appear only for conditioned specimens (RH50 and RH80).

The orientation sampling of the specimen influences the density of debonding, but also the kinetic of this mechanism. In the case of 0° specimens, the appearance and development of debonding is progressive with the stress increase, contrary to 90° specimens where their density soared.

3.3.2.3. Fibrillation. Although fibrillation is a matrix phenomenon, it results from the effect of neighbouring fibres. As presented in Fig. 25, the density of this mechanism highly depends on specimen orientation. 0° specimens show a low density of fibrillation. For this

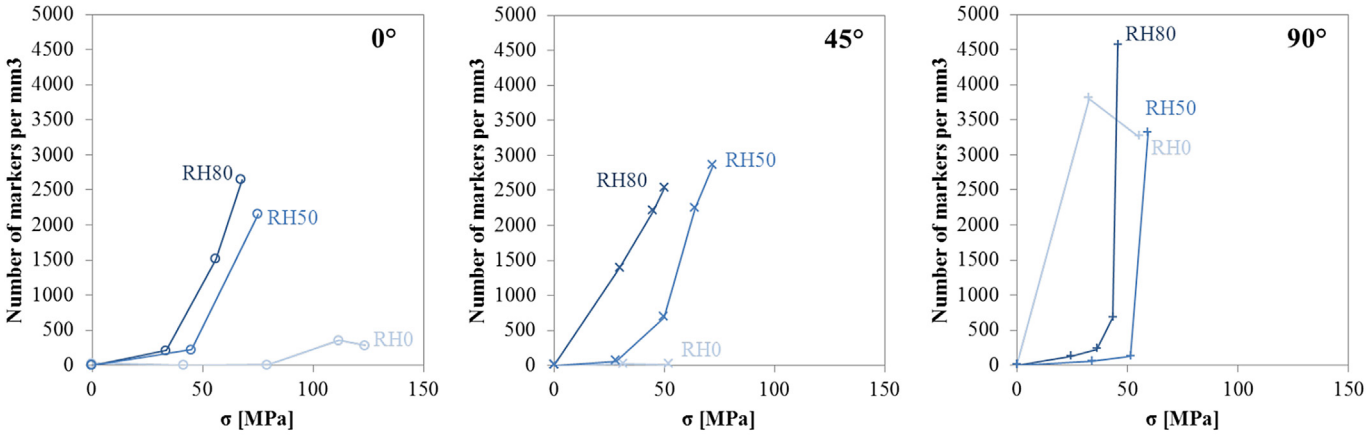

Fig. 21. Density of fibre failure.

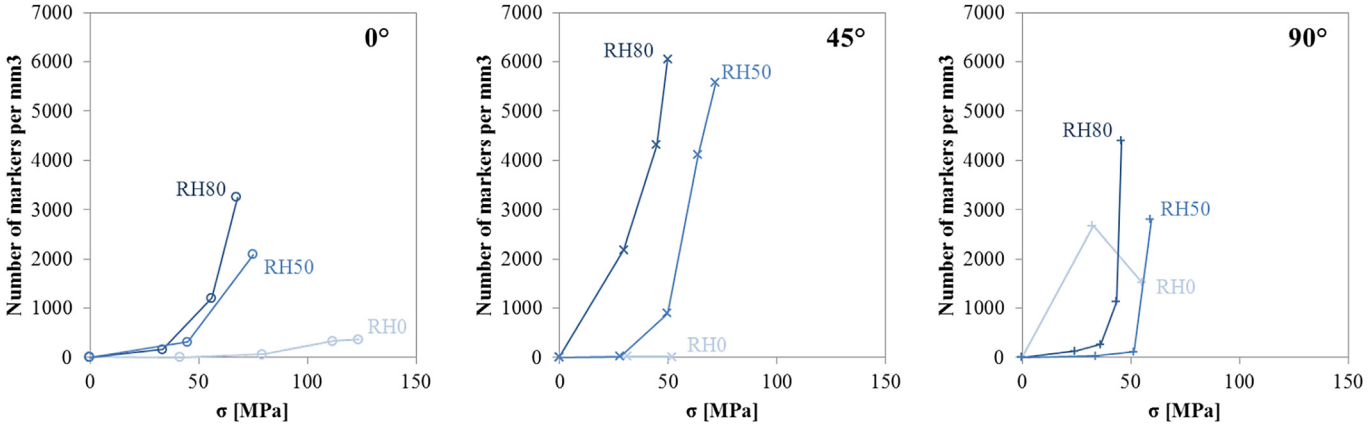

Fig. 22. Density of damage at fibre end.

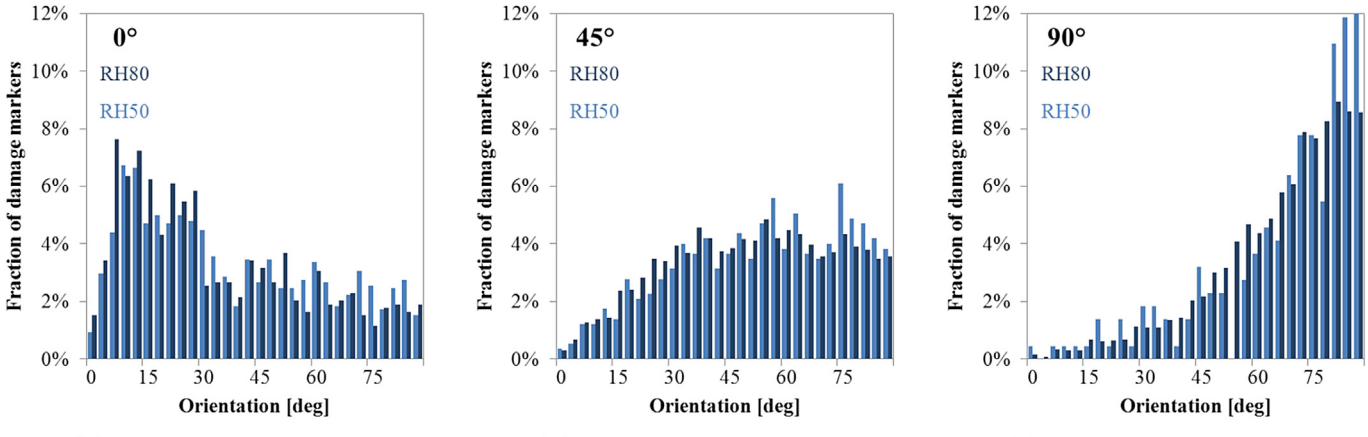

Fig. 23. Orientation of damage at fibre end.

orientation, the initiation stress level is linked with the conditioning of the specimen. Fibrillation in 45° and 90° specimens is initiated for the same range of stress levels. However, the conditioning significantly influences the magnitude of its density.

3.3.2.4. Cavitation. Although their small size, cavities are not the first to appear. These observations indicate that during *in situ* tensile tests, cavitation seems to be dependant of other mechanisms and not to be a first order mechanism (it only initiates close

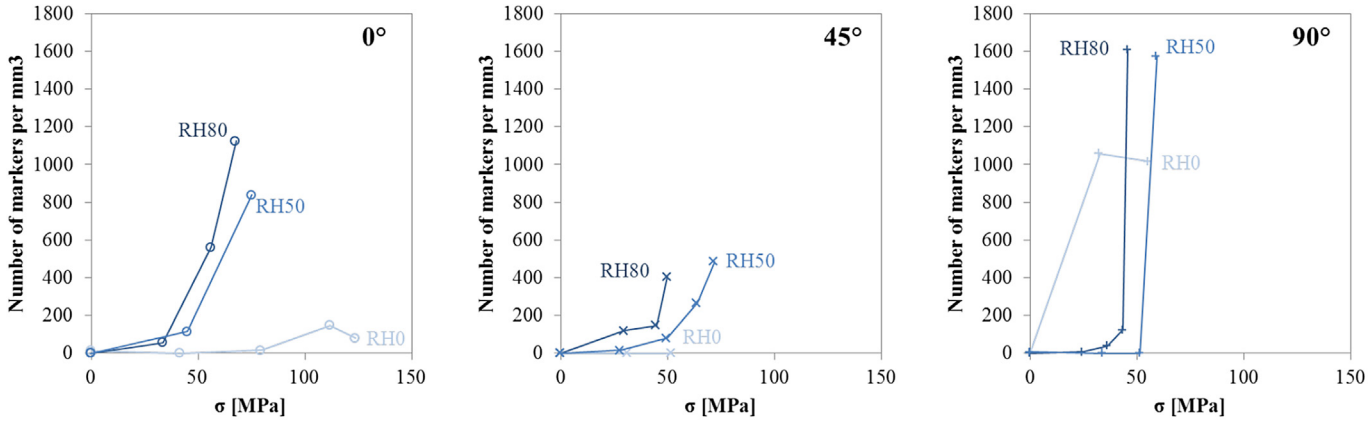

Fig. 24. Density of debonding.

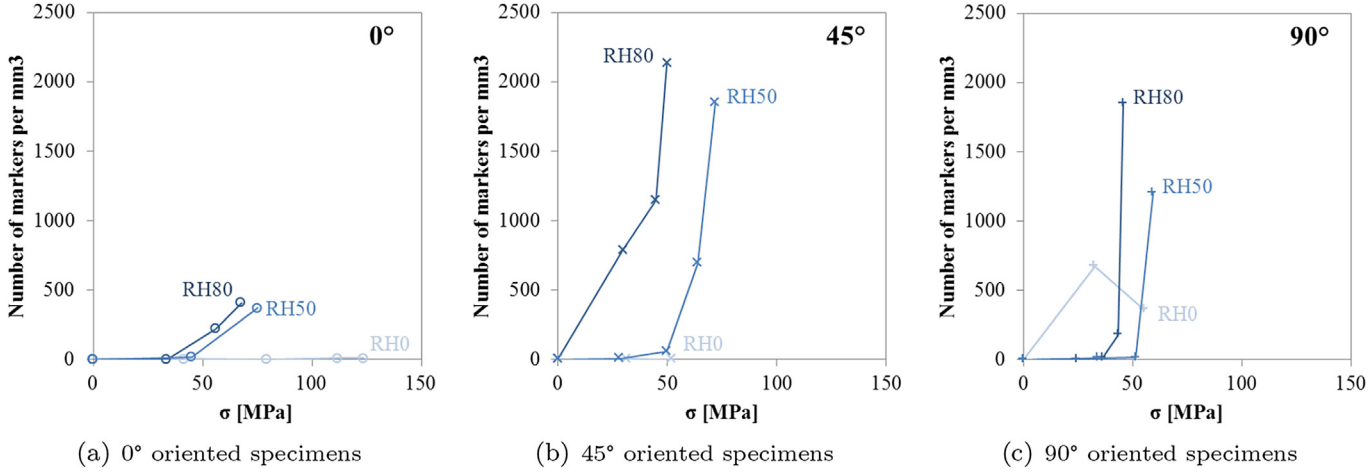

Fig. 25. Density of fibrillation.

to existing damaged zones). However, their high density allows to have a representative evolution of small markers in the gage length, as presented in Fig. 26 and this evolution is correlated to the global density.

3.3.2.5. Damage growth in the matrix. Damage growth in the matrix is the last activated mechanism during the tensile test. This mechanism is only observed at the very last stages of tensile tests for 45° or 90° specimens in the transition (RH50) or in rubbery state

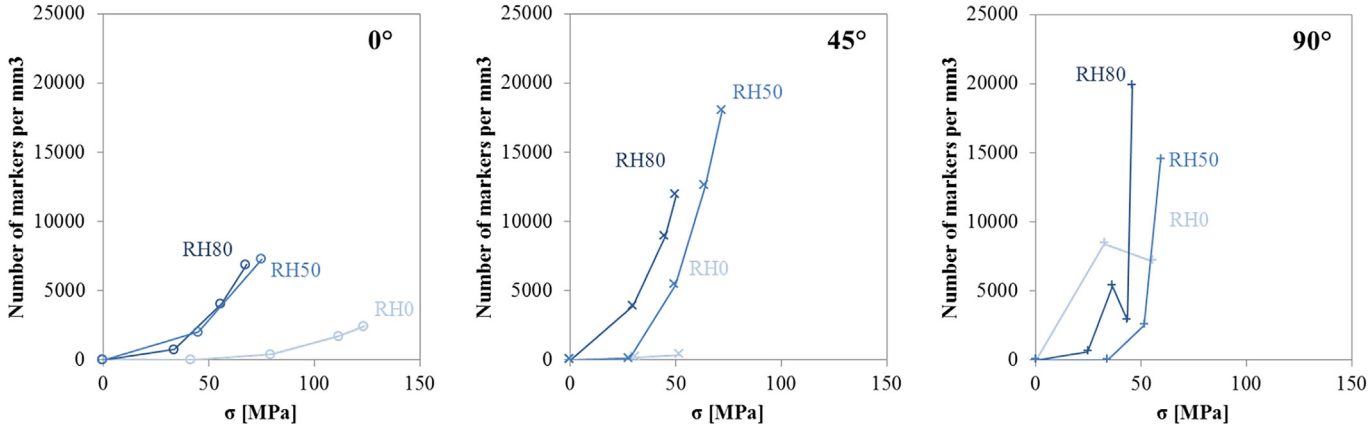

Fig. 26. Density of cavitation markers.

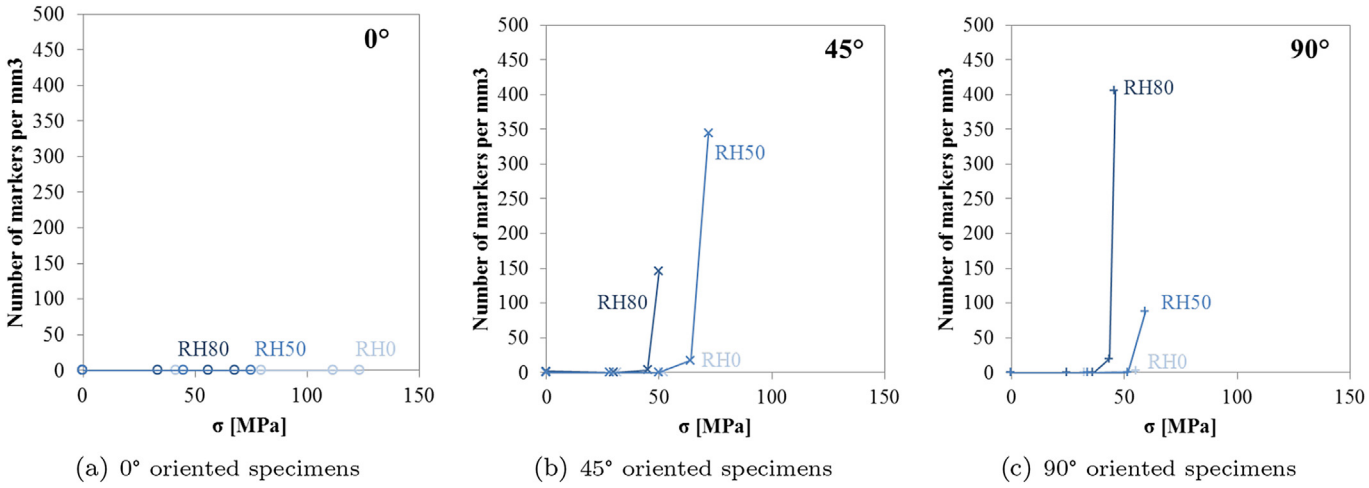

Fig. 27. Density of damage growth in the matrix.

(RH80), as illustrated in Fig. 27. The fact that this mechanism is not present in 0° oriented specimens and is not activated for dry specimens, indicates that the matrix is sensitive to conditioning and that the high ductility observed at the macroscopic scales of 45° and 90° specimens is associated with high local deformation and damage of the matrix at the microstructural level.

3.3.2.6. Volumetric proportions. Fig. 28 presents the proportions between volumes of each mechanism at 90% of the ultimate strength. For each specimen, it represents the volumetric proportions of damage markers according to whether they belong to the matrix, the fibres or the interface. In 0° specimens, damage is mainly governed by fibre failure and damage at fibre ends. For 45° specimens, half of the damage volume concerns damage in the matrix. The second half is increasingly attributed to interfacial damage when the humidity rate increases. Concerning 90° specimens, the proportions of matrix and interfacial damage are highly influenced by the relative humidity of the specimen. When the specimen is dry, interfacial damage is the most important. If the specimen is in its glassy transition, matrix damage represents half of the damage volume. When the specimen is in its rubbery state, the matrix damage constitutes two third of the damage volume whereas only one quarter is concerned by interfacial damage. It is then evidenced that ductile behaviour of the composite is fully linked with damage in the matrix.

3.4. Effect of relative humidity and orientation sampling on damage scenario

From observations at the microscopic scale, quantitative

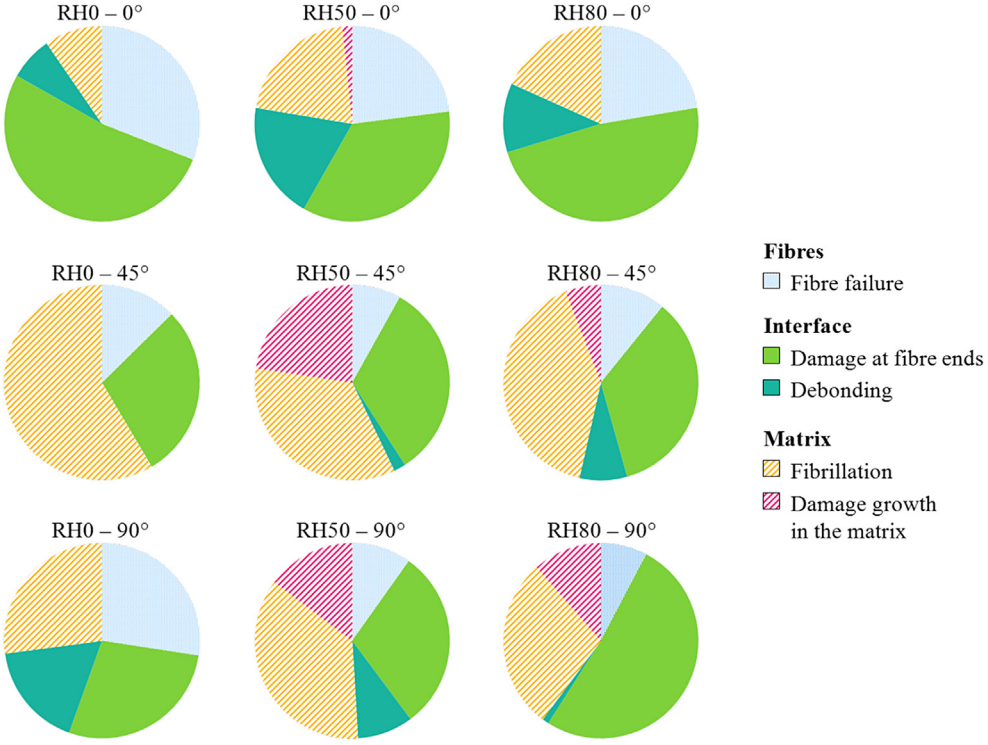

Fig. 28. Volumetric proportions of mechanisms at 90% of the UTS according to specimen orientation and conditioning.

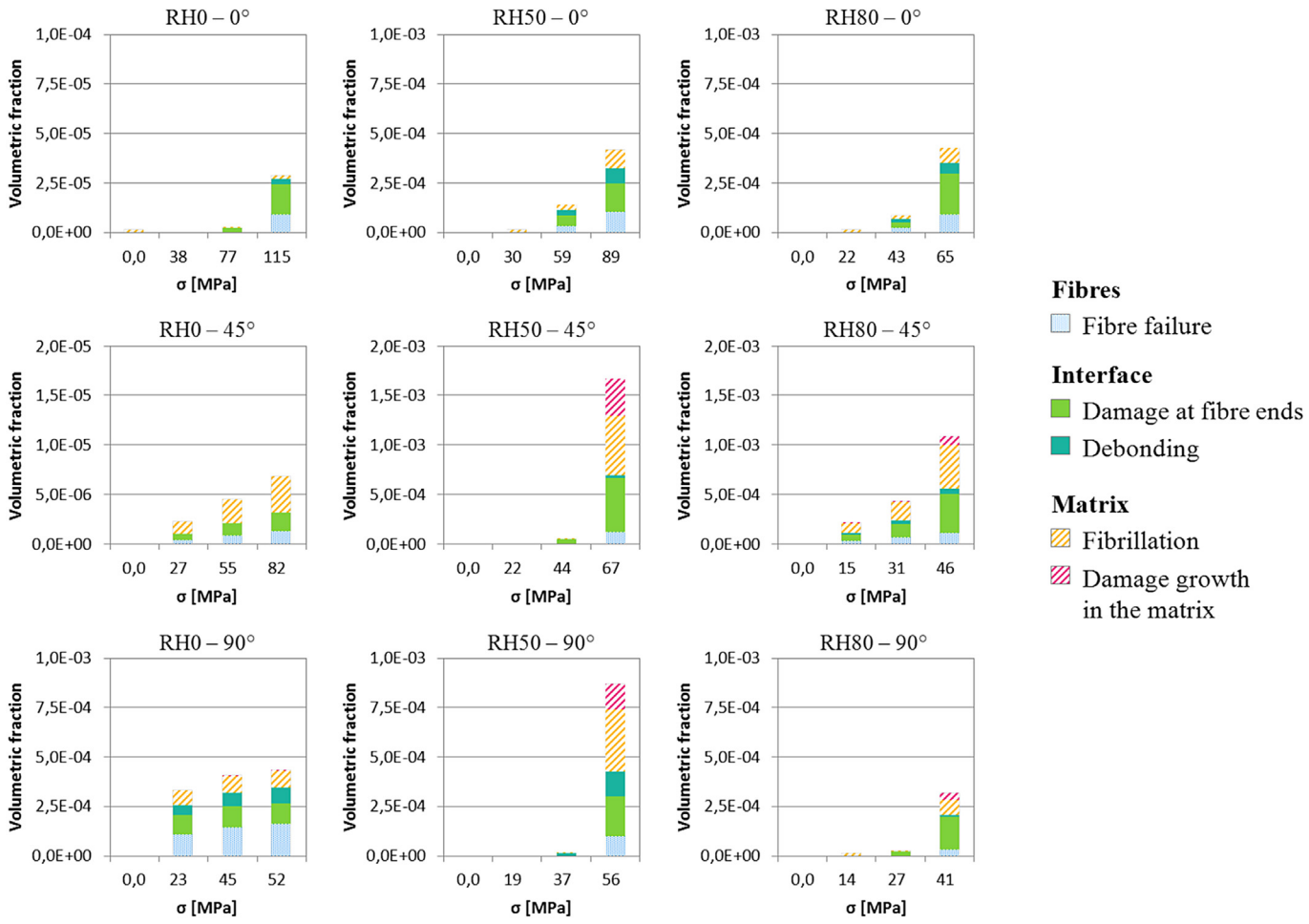

Fig. 29. Evolution of volumetric fraction per mechanism during tensile test (0%, 30%, 60% and 90% of the ultimate tensile strength) according to specimen orientation and conditioning.

information on density and volume of damage markers, it is possible to deduce a damage scenario for each specimen, sampled from 0°, 45° or 90° orientation from injected plates and conditioned at 0%, 50% or 80% of relative humidity. Damage progression in specimen can be divided in four steps.

1 The first step corresponds to damage initiation, at fibre ends or due to fibre failure. Orientation of the specimen can influence the fibre failure density, that is typically observed for 0° oriented fibre surrounded by fibres with different orientation. At this step neither orientation nor conditioning influence damage at fibre ends which is only due to the process (geometry and lack of sizing at fibre ends). However, the relative humidity may facilitate the detection of damage markers: whatever the specimen orientation, the damage markers become bigger with increase of relative humidity.

2 The intermediate step concerns the increase of density for fibre failure and damage at fibre ends. In the case of conditioned specimens (RH50 and RH80), new fibre ends resulting from fibre failure form markers corresponding to damage at fibre ends. A higher relative humidity also allows the growth of damage markers at fibre ends by stress triaxiality. According to the orientation of fibres (between 45° and 90° oriented fibres), damage at fibre end can initiate debonding. Also, this step sees the apparition of small cavities, linked with other damage markers.

3 During the advanced step, fibre failure and damage at fibre ends mechanisms keep developing. A critical stress in many confined zones between close fibres is probably reached, leading to a soar of debonding density. Fibrillation also appears at this step with densities first depending on relative humidity and then on specimen orientation: 45° oriented fibres being propitious to microcracks development.

4 The final step concerns the density increase of all described mechanisms, until the macroscopic failure of the specimen. In the case of conditioned specimens, with 45° or 90° orientation, damage markers are not only denser but get also larger. Fibre failures and damage at fibre ends growth in the matrix. Some debonding markers grow along all the fibre interface, joining both fibre ends and leading to markers with large volumes. Fibrillation keep occurring leading to coalescence of these markers. This damage growth in the matrix is linked with high deformation at the macroscopic scale.

Following these steps, Fig. 29 presents the evolution of the volumetric fraction of each damage mechanism at 0%, 30%, 60% and 90% of the ultimate strength.

4. Concluding remarks

Thanks to *in situ* X-ray microtomography tensile tests, 3D pictures of the gage length of specimens in different conditions of humidity and fibre orientation have been obtained at different stages from the first steps to the failure of the specimen. Observations of these pictures have been combined with quantitative analyses to describe the six different damage mechanisms

identified in the bulk of the material: fibre failure, damage at fibre ends, debonding, cavitation, fibrillation and damage growth in the matrix. The main effects of specimen conditioning is the increase of both density and volume of damage markers, particularly matrix damage. Differences of damage mechanisms due to orientation sampling are: 0° oriented specimens provide numerous fibres with an orientation more susceptible to break whereas 45° and 90° oriented specimens are more dependent on the matrix behaviour. In this case, a ductile behaviour is observed.

Acknowledgement

The authors gratefully acknowledge Solvay Engineering Plastics for supporting this work and for providing specimens. This work was performed in the framework of the DURAFIP project (FUI project supported by Oseo).

References

[1] Bernasconi A, Davoli P, Basile A, Filippi A. Effect of fibre orientation on the fatigue behaviour of a short glass fibre reinforced polyamide-6. Int J Fatigue 2007;29:199–208.
[2] Zhou Y, Mallick PK. Fatigue performance of an injection-molded short E-glass fiber-reinforced polyamide 6,6. I. Effects of orientation, holes, and weld line. Polym Compos 2006;27:230–7.
[3] Tanaka K, Kitano T, Egami N. Effect of fiber orientation on fatigue crack propagation in short-fiber reinforced plastics. Eng Fract Mech 2014;123:44–58.
[4] Rolland H, Saintier N, Robert G. Damage mechanisms in short glass fibre reinforced thermoplastic during in situ microtomography tensile tests. Compos Part B 2016;90:365–77.
[5] Sato N, Kurauchi T, Sato S, Kamigaito O. Mechanism of fracture of short glass fibre-reinforced polyamide thermoplastic. Jounal Mater Sci 1984;19:1145–52.
[6] Sato N, Kurauchi T, Sato S, Kamigaito O. Microfailure behaviour of randomly dispersed short fibre reinforced thermoplastic composites obtained by direct sem observation. Jounal Mater Sci 1991;26:3891–8.
[7] Horst JJ, Spoormaker JL. Mechanisms of fatigue in short glass fiber reinforced polyamide 6. Polym Eng Sci 1996;36(22):2718–26.
[8] Horst JJ, Spoormaker JL. Fatigue fracture mechanisms and fractography of short-glassfibre-reinforced polyamide 6. J Mater Sci 1997;32(14):3641–51.
[9] Arif MF, Saintier N, Meraghni F, Fitoussi J, Chemisky Y, Robert G. Multiscale fatigue damage characterization in short glass fiber reinforced polyamide-66. Compos Part B 2014;61:55–65.
[10] Arif MF, Meraghni F, Chemisky Y, Despringre N, Robert G. In situ damage mechanisms investigation of pa66gf30 composite: effect of relative humidity. Compos Part B 2014;58:487–95.
[11] Barbouchi S, Bellenger V, Tcharkhtchi A, Castaing Ph, Jollivet T. Effect of water on the fatigue behaviour of a pa66/glass fibers composite material. J Mater Sci 2007;42(6):2181–8.
[12] Launay A, Marco Y, Maitournam MH, Raoult I. Modelling the influence of temperature and relative humidity on the time-dependent mechanical behaviour of a short glass fibre reinforced polyamide. Mech Mater 2013;56:1–10.
[13] Salvo L, Cloetens P, Maire E, Zabler S, Blandin JJ, Buffiere J-Y, et al. X-ray micro-tomography an attractive characterisation technique in materials science. Nucl Instrum Methods Phys Res B 2003;200:273–86.
[14] Buffiere J-Y, Proudhon H, Ferrie E, Ludwig W, Maire E, Cloetens P. Three dimensional imaging of damage in structural materials using high resolution micro-tomography. Nucl Instrum Methods Phys Res B 2005;238:75–82.
[15] Cosmi F, Bernasconi A. Micro-ct investigation on fatigue damage evolution in short fibre reinforced polymers. Compos Sci Technol 2013;79:70–6.
[16] Ayadi A, Nouri H, Guessama S, Roger F. An original approach to assess elastic properties of a short glass fibre reinforced thermoplastic combining x-ray tomography and finite element computation. Compos Struct 2015;125:277–86.
[17] Cosmi F, Ravalico C. Threshold identification for micro-tomographic damage characterisation in a short-fibre-reinforced polymer. Strain 2015;51:171–9.
[18] Horst JJ, Salienko NV, Spoormaker JL. Fibre-matrix debonding stress analysis for short fibre-reinforced materials with matrix plasticity, finite element modelling and experimental verification. Compos Part A 1998;29:525–31.
[19] Klimkeit B, Castagnet S, Nadot Y, El Habib A, Benoit G, Bergamo S, et al. Fatigue damage mechanisms in short fiber reinforced PBT+PET GF30. Mater Sci Eng A 2011;528(3):1577–88.